PCCP

PAPER

Dispersion interactions in silicon allotropes†

Antti J. Karttunen,*[a] Denis Usvyat,[b] Martin Schütz[b] and Lorenzo Maschio*[c]

Cite this: *Phys. Chem. Chem. Phys.*, 2017, **19**, 7699

Received 28th December 2016,
Accepted 17th February 2017

DOI: 10.1039/c6cp08873b

rsc.li/pccp

van der Waals interactions are known to play a key role in the formation of weakly bound solids, such as molecular or layered crystals. Here we show that the correct quantum-chemical description of van der Waals dispersion is also essential for a correct description of the relative stability between purely covalently-bound solids like silicon allotropes. To this end, we apply periodic local MP2 and DFT with Grimme's empirical −D3 correction to 11 experimentally determined or yet hypothetical crystalline silicon structures, including the most recently discovered silicon allotropes. Both methods provide similar energy ordering of the polymorphs, which, at the same time, noticeably deviate from the order predicted by standard DFT without an appropriate description of the van der Waals dispersion.

Introduction

Novel allotropes of the chemical elements are of great scientific and technological interest. For example, the step-wise discovery of carbon fullerenes,[1] carbon nanotubes,[2] and graphene[3] has each time opened up a completely new research field of increasing proportions. There are also significant ongoing experimental and computational efforts towards the discovery of new allotropes for the heavier group 14 elements silicon and germanium. In the case of silicon, its fundamental technological role as the key material in microelectronic and photovoltaic technologies is a major driving force for the research towards novel allotropes. In particular, the discovery of direct bandgap silicon allotropes that can be prepared in bulk quantities could result in improved silicon-based photovoltaic or optoelectronic applications, depending on the magnitude of the band gap. Important examples of well-characterized silicon allotropes are Si(*cF*136) (silicon clathrate II),[4,5] and the other recently synthesized open-framework allotrope Si(*oC*24).[6] Of these two open-framework allotropes the *cF*136 structure has also been obtained for germanium.[7] Neither Si(*cF*136) nor Si(*oC*24) possess a direct band gap, but their controlled preparation *via* vacuum treatment of the binary precursors Na_xSi_{136} and Na_4Si_{24} illustrates an important synthetic strategy for the discovery of novel silicon and germanium allotropes.

A large number of previous computational studies have focused on existing and hypothetical allotropes of silicon. Because tetrahedrally coordinated group 14 atoms such as silicon can form a vast number of different types of networks, a systematic classification of the possible network topologies is of utmost importance.[8] A highly efficient way to analyze the network topologies is the TOPOS software suite,[9] which also includes structural databases that can be used to assess whether a certain topology is really a novel one or if it has already been discovered. Another important resource in this field is the Reticular Chemistry Structure Resource,[10] which provides thousands of already known network topologies. Finally, many tetrahedrally coordinated carbon allotropes predicted in the literature are also relevant for silicon, and the recently introduced Samara Carbon Allotrope Database provides convenient access to hundreds of network topologies relevant for tetrahedrally coordinated group 14 elements.[11]

Due to the vast number of hypothetical silicon allotropes proposed in the recent literature and provided in the above-mentioned structural databases, we will not review all of them here. For those interested in a deeper survey of the existing allotropes, Bromley *et al.* have provided an excellent and extensive review of low-density allotropy in silicon.[12] Low-density allotropes and the structural principles of silicon clathrate frameworks have also been discussed in ref. 13. Finally, a review of more recent work on silicon allotropes is included in a paper that also provides guidelines for deriving Si allotropes in a chemistry-inspired fashion from the diamond structure.[14] The number of hypothetical silicon allotropes is expected to increase steadily as novel strategies are adopted for discovering them. *Ab initio* random structure searches and particle swarm methods are some examples of the new strategies.[15,16] Another very fruitful strategy is to exploit the topologies known for zeolites.[17–20]

Practically all computational studies on existing and hypothetical silicon allotropes so far have been carried out using standard density functional theory (DFT) methods, that is,

[a] *Department of Chemistry and Materials Science, Aalto University, FI-00076 Aalto, Finland. E-mail: antti.j.karttunen@iki.fi*
[b] *Institut für Chemie, Humboldt Universität zu Berlin, Brook-Taylor-Str. 2, D-12489 Berlin, Germany*
[c] *Dipartimento di Chimica, and NIS (Nanostructured Interfaces and Surfaces) centre, Universitá di Torino, via, Giuria 5, Torino I-10125, Italy. E-mail: lorenzo.maschio@unito.it*

† Electronic supplementary information (ESI) available. See DOI: 10.1039/c6cp08873b

with either LDA, GGA, or hybrid exchange correlation functionals. A common problem of standard DFT functionals is that they cannot capture van der Waals-dispersion interactions, unless the dispersion correction is added to the DFT energy.[21,22] To our knowledge, the role of dispersion interactions in the energetics of tetrahedrally coordinated silicon allotropes has been neglected so far. While dispersion interactions play a key role in structural chemistry of molecular crystals,[21–23] they are typically considered to be less important for bulk solids with covalent or ionic bonding. However, previous work on bulk TiO_2 or BN polymorphs has clearly illustrated that dispersion interactions can be important also for network-type bulk materials and need to be taken into account to obtain the experimentally known energy ordering of topologically different polymorphs.[24–26] Indeed, two-body dispersion is always an attractive force, which in bulky systems can accumulate to a sufficiently large contribution to influence even the relative stabilities of covalently bound polymorphs.

We note at this point that some standard functionals (*e.g.* LDA, PBE, or PBEsol) deliver artificial non-electrostatic binding between two closed-shell systems, which can to a certain extent effectively substitute the van der Waals interaction. However, this fortuitous error compensation can only ''work'' in small systems, since this fictitious binding has an exponential rather than the genuine R^{-6} decay of the van der Waals dispersion. Therefore, the effect of accumulated long-range dispersion in bulky systems cannot be captured in this way. In order to overcome this problem, in the past few decades several DFT-based approaches appeared that include van der Waals interaction. The presently most popular technique is abovementioned Grimme's empirical correction D.[21] There are also more rigorous ways of treating dispersion within the DFT framework,[22,27–31] which however are usually computationally much more demanding than standard DFT.

An alternative to DFT is the *ab initio* wave-function methodology. These methods can capture dispersion as well as other types of interactions in a balanced and non-empirical way. Furthermore, these techniques form methodological hierarchies, allowing for a systematic improvement of the accuracy of the results. The problem of such methods is their computational cost, which, especially in solids, can become prohibitively high. Nevertheless, low order quantum chemical methods, such as MP2[32,33] or the Random Phase Approximation (RPA),[34,35] are available in the periodic form and can be applied for relatively complex systems. Higher order corrections can be calculated using fragment-based approaches.[36–40] The most advanced hierarchical wavefunction-based techniques already challenge the accuracy of experimentally determined lattice[41] or adsorption energies.[42]

In this work we investigate dispersion interactions in different types of silicon allotropes to shed light on the stability trends of the allotropes. By applying the Orbital-Specific Virtuals (OSV) LMP2 approach[43] recently implemented in the CRYSCOR code,[32] we carry out a systematic comparison of dispersion interactions in different silicon topologies without any empirical parametrization. We also compare our results with standard and dispersion-corrected DFT methods and demonstrate that the dispersion interactions have a significant effect on the predicted stabilities of several low-density allotropes of silicon. van der Waals dispersion in a silicon clathrate framework containing noble gas guest atoms has been investigated by some of us using periodic LMP2 and dispersion-corrected DFT earlier.[44] However, that study focused on the host–guest interactions and included only a single network topology. In the present study, we shift our focus on dispersion within the covalent networks themselves and its role in their relative energetics.

Computational methods

The silicon allotropes were investigated using two different types of quantum chemical methods, which are, density functional theory (DFT) and local second-order Møller–Plesset perturbation theory (LMP2).[45] The DFT calculations were carried out using the CRYSTAL14 program package.[46] In addition to the standard hybrid PBE0 functional, we also applied Grimme's empirical DFT-D3 dispersion correction with Becke–Johnson damping (PBE0-D3).[47–50] Both LMP2 and DFT calculations were carried out using a localized Gaussian-type basis set of triple-zeta-valence + double polarization (TZVPP[44,51]) quality. The Monkhorst–Pack-type *k*-point grids used for sampling the reciprocal space of each structure are listed in the Results and discussion section.[52] The geometries of all studied structures were fully optimized using both PBE0 and PBE0-D3 functionals and for both functionals the relative energy at the respective local minimum is used in the comparisons. Full structural data and detailed specification of the computational parameters and the basis set can be found in the ESI.† All studied structures have been confirmed previously to be true local minima either with DFT-GGA or hybrid DFT methods (see the Results and discussion section for references). The three-body (ABC) contribution to the D3 dispersion[53] correction was tested on a few single-point structures at the PBE0 minimum, but the effect of the three-body contribution on relative stabilities does not appear to be significant. For example, the relative energy of the *hP*8 structure in comparison to the *cF*8 structure did not change, while the relative energy of the *cF*136 structure decreased by 2.5%.

The LMP2 calculations were carried out with a development version of the CRYSCOR software,[32] which implements orbital-specific virtuals (OSVs) to represent the truncated pair-specific virtual space.[43] In the OSV-LMP2 formalism, it is not necessary to manually define excitation domains for the virtual space as in the previous implementation based on projected atomic orbitals (PAO-LMP2). The OSV-LMP2 straightforwardly enables the calculation of smooth potential energy surfaces and relative energies of structural frameworks with different topologies.[40,43] The Hartree–Fock reference wavefunction and the localized valence-space Wannier functions (WFs) necessary for the LMP2 procedure were obtained with CRYSTAL14. In the LMP2 calculations, we utilized the direct-space density-fitting technique for computing the two-electron four-index integrals.[54]A Poisson/Gaussian-type

auxiliary basis set[55,56] corresponding to the triple-zeta-valence orbital basis set[57] was employed for density-fitting.

Due to the lack of analytical gradients, full geometry optimizations of the studied structures were not yet computationally feasible at the LMP2 level. Instead, we performed single-point energy calculations at the geometries optimized with the DFT methods. A potential energy scan for the lattice constant of α-Si showed that an optimal LMP2 lattice constant of 5.43 Å is practically identical to the PBE0 lattice constant, while the PBE0-D3-optimized lattice constant has a slightly smaller value of 5.39 Å (see the ESI† for details on the LMP2 potential energy scan). The experimental value of the lattice constant at 6.4 K is 5.430 Å.[58,59] The low-temperature value is in fact close to the room temperature value of 5.431 Å because α-Si shows negative thermal expansion up to about 170 K. The LMP2/TZVPP relative energies reported here have been calculated at the PBE0 geometries, but the relative LMP2 energies obtained at the PBE0-D3 geometries are very similar. We note that in a previous study utilizing DFT-PBE with semiempirical dispersion corrections, the effect of the dispersion correction on the lattice constant of α-Si was four times smaller in comparison to the difference arising from the D3 correction.[60]

Results and discussion

The silicon allotropes studied in this work are described in Table 1 and Fig. 1–3. The energetically most favorable silicon allotrope (*cF*8) α-Si is used as the reference to investigate the relative energies of the other ten allotropes. These have been shown to be among the energetically most favorable structures in previous computational studies carried out typically with DFT-LDA, DFT-PBE, and DFT-PBE0 methods that cannot properly describe weak dispersion interactions. Some of the silicon allotropes studied here have been synthesized experimentally (*hP*4, *oC*24, *cF*136), while all others, yet hypothetical, show some close relation to experimentally known materials (some are known for Ge, but not for Si). We note that several silicon allotropes, which do not show any direct relationship with experimentally known materials, have also been predicted recently.[15,61] They show rather low relative energy because the structures incorporate the strain-free diamond lattice as a building block.

In the following, we denote the individual silicon allotropes under study by their Pearson symbols. We briefly discuss their network topologies in the captions of Fig. 1–3. The full descriptions of their structural characteristics can be found in the original references cited in Table 1. The network topologies of most of the structures are described in full detail in the RCSR database or can be obtained with the help of the TOPOS program.[8,10]

The relative energies ΔE predicted for the studied silicon allotropes are listed in Table 2 and illustrated in Fig. 4. The *cF*8 structure is used as the reference with $\Delta E = 0.0$ kJ mol^{-1} Si^{-1}. The energy ordering of the allotropes obtained at the PBE0/TZVPP level of theory is in line with previous computational studies carried out with DFT-GGA and hybrid DFT methods,[12–14,17] even though no previous paper includes exactly the same set of allotropes as discussed here. However, the energy ordering of the allotropes shows some significant changes when dispersion interactions are taken into account either with the PBE0-D3 or

Table 1 Silicon allotropes included in this study. The structures are ordered according to their relative energy ΔE at the LMP2/TZVPP level (see below) from the most to the least stable structure

Pearson[a]	Name(s)[b]	Space group	a[c] (Å)	b[c] (Å)	c[c] (Å)	k-Grid[d]	Notes
*cF*8	Alpha (α)/3C	$Fd\bar{3}m$	5.43			12 × 12 × 12	Diamond structure. Most stable Si allotrope under STP conditions.
*hP*8	4H	$P6_3/mmc$	3.83		12.59	12 × 12 × 4	Hexagonal polytype of 3C. 4H-Ge has been synthesized as a bulk material starting from *m-allo*-Ge.[62,63]
*hP*4	2H	$P6_3/mmc$	3.83		6.32	12 × 12 × 6	Hexagonal polytype of 3C. 2H-Si has been fabricated on GaP nanowire templates.[64]
*tP*12	cdp/T12	$P4_2/ncm$	5.19		9.24	8 × 8 × 4	Hypothetical allotrope, topology the same as in CdP_2.[16,65]
*oP*32	GAa4	*Pbcm*	7.85	11.29	7.45	4 × 4 × 4	The most stable building block of stacking-faulted *m-allo*-Ge (synthesized as a bulk material structure starting from Li_7Ge_{12}).[17,63]
*hP*6	unj/NGS	$P6_122$	5.44		5.08	8 × 8 × 8	Hypothetical allotrope, topology the same as for the Ga–Sn network in $NaGaSn_5$.[17,66]
*tP*24	tum1	$P4_2/nmc$	7.42		9.15	6 × 6 × 4	Hypothetical allotrope, topology the same as for the B–Si network in $LiBSi_2$.[67]
*oC*24	CAS	*Cmcm*	3.82	10.68	12.66	8 × 8 × 4	Has been synthesized from Na_4Si_{24}.[68]
*cF*136	Clathrate II	$Fd\bar{3}m$	14.65			4 × 4 × 4	Has been synthesized from Na_xSi_{136},[4,5] also known for Ge.[7]
*cI*46	Clathrate VIII	$I\bar{4}3m$	10.04			4 × 4 × 4	Hypothetical allotrope, experimentally known in type-VIII Ge and Sn clathrates.[13,69,70]
*cP*46	Clathrate I	$Pm\bar{3}n$	10.16			4 × 4 × 4	Hypothetical allotrope, experimentally known in Na_8Si_{46} type-I clathrate.[13,69,70]

[a] Pearson symbol of the allotrope, including the Bravais lattice and the number of atoms in the crystallographic unit cell. For the *cF*8, *oC*24, *cF*136, and *cI*46 structures the number of atoms in the primitive cell is 2, 12, 34, and 23, respectively. [b] Names/codes used for the structure in the literature (see Notes). [c] Lattice parameters of the structure obtained at the PBE0/TZVPP level of theory. [d] Monkhorst–Pack-type k-point grid used for sampling the reciprocal space.

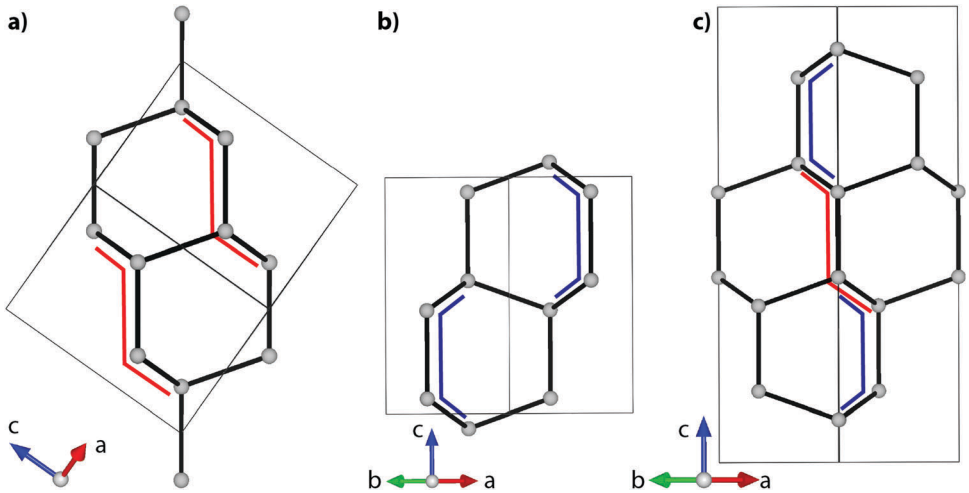

Fig. 1 Simple silicon allotropes that are polytypes of the diamond structure. (a) *cF*8 (α-Si/3C polytype); (b) *hP*4 (2H polytype); (c) *hP*8 (4H polytype). The *cF*8 structure has been oriented to emphasize the structural connection to the hexagonal polytypes. The red lines denote six-membered rings in the chair conformation, while the blue lines denote six-membered rings in the slightly more strained boat conformation. The least strained 3C polytype possesses only six-membered rings in the chair conformation.

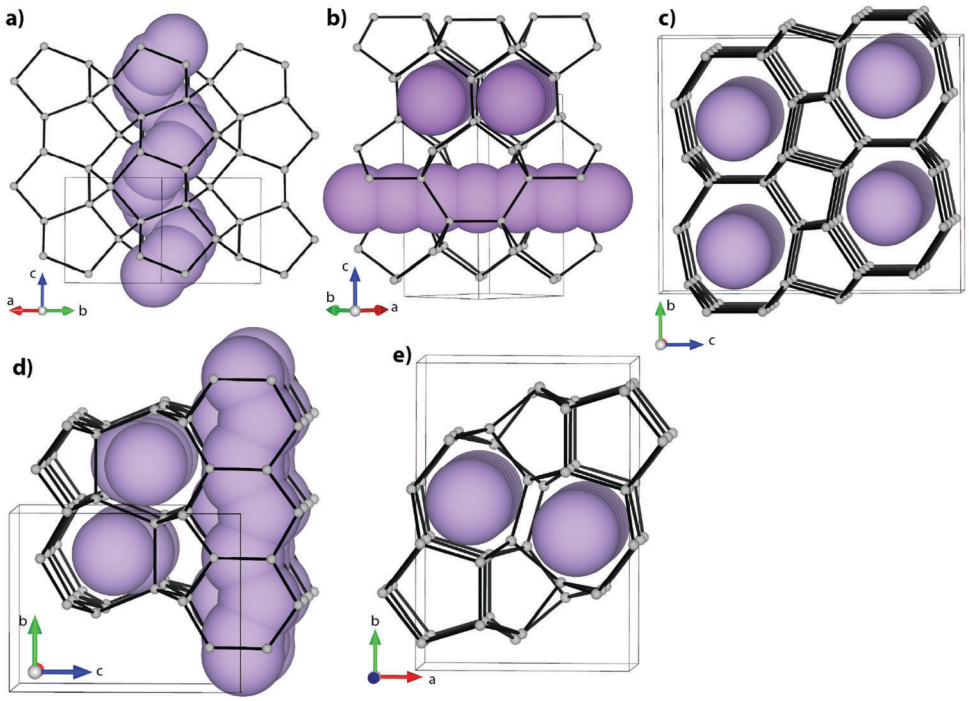

Fig. 2 Silicon allotropes that are less dense than the diamond polytypes shown in Fig. 1. All structures possess channels highlighted by the violet space-filling balls. (a) *hP*6 (unj/NGS); (b) *tP*12 (cdp/T12) (c) *oC*24 (CAS); (d) *tP*24 (tum1); (e) *oP*32 (GAa4). *hP*6 contains helical (chiral) channels in one direction, while in *tP*12 similar helical channels are stacked in a perpendicular fashion along the *c* axis. In *oC*24, *tP*24, and *oP*32 the channels highlighted here are formed by eight-, seven-, and seven-membered rings, respectively. All three allotropes also possess smaller channels formed by five-membered rings. In *tP*24, the larger channels run in a perpendicular fashion. The structures *hP*6, *tP*12, and *tP*24 can actually be derived by slicing and re-connecting the *cF*8 diamond structure and the structural characteristics of these allotropes have been recently described in detail.[14]

the LMP2 method. The relative energies of the allotropes with lowest densities clearly increase in comparison to the denser allotropes when dispersion interactions are taken into account. For example, for the lowest-density allotrope, that is, the *cF*136 clathrate, ΔE increases from 7.2 kJ mol^{-1} Si^{-1} (PBE0) to 12.6 kJ mol^{-1} Si^{-1} (PBE0-D3) or 13.5 kJ mol^{-1} Si^{-1} (LMP2). The silicon atoms are bound in a similar tetrahedral fashion in all studied allotropes, but in denser structures the next-nearest neighbors are closer than in lower-density structures with cavities or channels, resulting in stronger dispersion interactions. The correlation between the dispersion interactions is clearly seen in Fig. 5, which shows the difference between $\Delta E_{\mathrm{PBE0\text{-}D3}}$ and

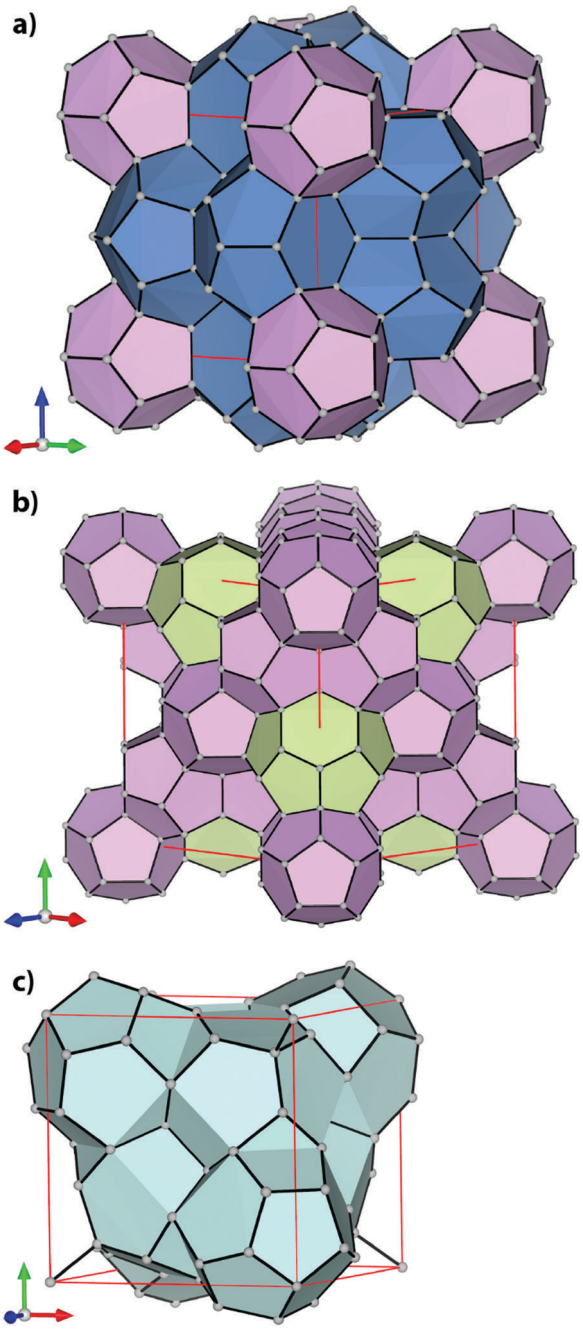

Fig. 3 The least dense silicon allotropes studied here: clathrate frameworks composed of polyhedral cages. (a) *cP*46 (Clathrate I) composed of 20-membered (violet) and 24-membered (blue) cages; (b) *cF*136 (Clathrate II) composed of 20-membered (violet) and 28-memberd (green) cages; (c) *cI*46 (Clathrate VIII) composed of 23-membered cages. The structural principles of the studied clathrate frameworks have been described in detail elsewhere.[13]

Table 2 Predicted relative energies of the studied silicon allotropes. The structures are ordered according to their relative energy ΔE at the LMP2/TZVPP level

		ΔE^c (kJ mol^{-1} Si^{-1})		
Pearson[a]	Density[b] (g cm^{-3})	PBE0	PBE0-D3	LMP2
*cF*8	2.316	0.0	0.0	0
*hP*8	2.320	0.3	0.4	1.2
*hP*4	2.319	1.0	1.1	1.9
*tP*12	2.245	5.7	7.1	7.6
*oP*32	2.250	7.6	8.9	8.5
*hP*6	2.137	6.9	10.3	10.6
*tP*24	2.210	9.4	11.5	10.6
*oC*24	2.157	10.3	13.1	12.4
*cF*136	2.010	7.2	12.6	13.5
*cI*23	2.112	10.1	14.0	13.6
*cP*46	2.036	8.5	13.5	14.1

[a] Pearson symbol of the silicon allotrope (see Table 1). [b] Density of the allotrope (PBE0/TZVPP geometry). [c] Relative energy of the allotrope, obtained as $\Delta E = E(\text{allotrope})/n - E(cF8)/2$, where n is the number of atoms in the primitive cell of the allotrope ($n = 2$ for *cF*8). The PBE0 and PBE0-D3 energies have been obtained for PBE0 and PBE0-D3 optimized structures, respectively. The LMP2 energies are for PBE0-optimized structures (see Computational details)

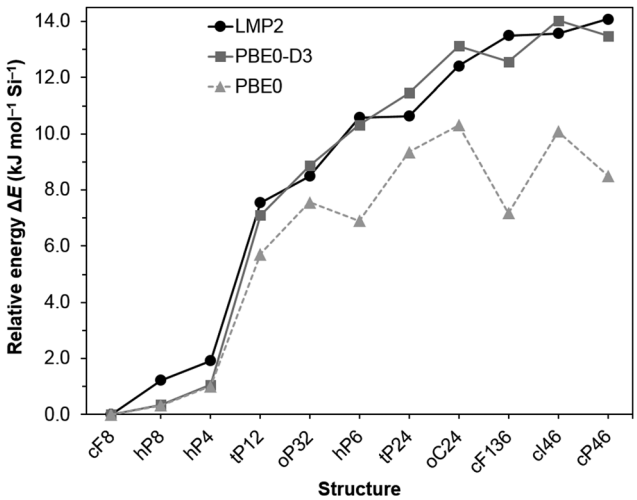

Fig. 4 Relative energies of the studied silicon allotropes obtained with PBE0, PBE0-D3, and LMP2 methods (see Table 2 for details). The PBE0 and PBE0-D3 energies have been obtained for PBE0 and PBE0-D3 optimized structures, respectively. The LMP2 energies are for PBE0-optimized structures (see Computational details).

ΔE_{PBE0} plotted as a function of density of the individual silicon allotropes (the densest *cF*8 allotrope has the largest absolute D3 contribution per atom and $\Delta E_{\text{PBE0-D3}} - \Delta E_{\text{PBE0}}$ increases for the less dense allotropes). Since the D3 dispersion coefficients by construction remain the same for all the crystals under study, the magnitude of the D3 contribution to the energy per one Si atom has to grow linearly with the increase of the density, which is also evident from Fig. 5. Though two-body dispersion is a weak attractive force, it is relatively long-ranged: it decays with the inverse sixth power of the distance between the interacting fragments. Yet due to the 3D packing, the number of formal fragments in a solid, separated by a certain distance R from a given center, grows quadratically with this distance. Hence, dispersion interactions have effectively a much larger range and are of greater importance in crystals compared to molecular systems. As the presented results demonstrate, the excess in dispersion in more compact structures is already sufficient to influence the relative stability between the silicon allotropes with different topologies.

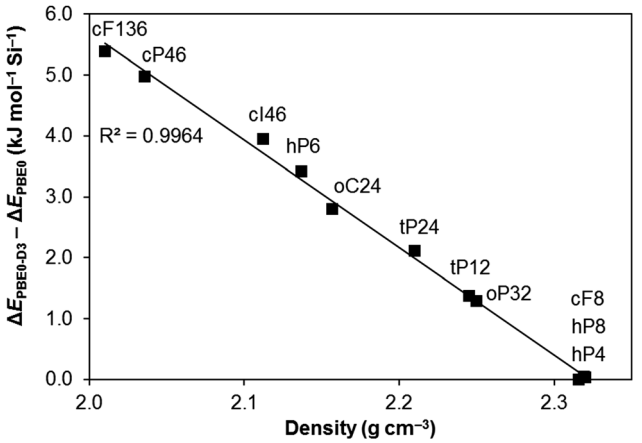

Fig. 5 The difference between $\Delta E_{PBE0\text{-}D3}$ and ΔE_{PBE0} plotted as a function of density for the studied silicon allotropes. Note that in this double difference formula, $\Delta E_{PBE0\text{-}D3}$ and ΔE_{PBE0} are by definition zero for the densest allotrope Si-cF8 (see the caption of Table 2 for the definition of ΔE).

The PBE0-D3 and LMP2 methods yield rather similar relative energies. The D3 correction does not capture the influence of the topology on the dispersion coefficients, which depend only on the atomic species. The LMP2 treatment of dispersion, on the other hand, is rigorous in this respect. However, since both methods provide the same general pattern for the relative stability as a function of the density, the influence of the structure on the dispersion coefficients seems not to be substantial (at least for the allotropes considered in this study). Nevertheless, the predicted energy ordering does show some differences. In particular, the energy ordering changes from $\Delta E(cF136) < \Delta E(oC24)$ to $\Delta E(oC24) < \Delta E(cF136)$ when comparing PBE0-D3 to LMP2. Both of these allotropes have been synthesized (see Table 1), demonstrating that the energy orderings discussed here are relevant for experimentally known species. Interestingly, the dense *hP*8 and *hP*4 allotropes closely related to the *cF*8 reference structure illustrate one clear difference between the $\Delta E_{PBE0\text{-}D3}$ and ΔE_{LMP2} values. For PBE0-D3, $\Delta E(hP8)$ = 0.4 kJ mol^{-1} Si^{-1} and $\Delta E(hP4)$ = 1.1 kJ mol^{-1} Si^{-1}, which are very close to the PBE0 values of 0.3 and 1.0 kJ mol^{-1} Si^{-1}, respectively. For comparison, the LMP2 values are $\Delta E(hP8)$ = 1.2 kJ mol^{-1} Si^{-1} and $\Delta E(hP4)$ = 1.9 kJ mol^{-1} Si^{-1}, suggesting a much larger importance of dispersion interactions for the relative energetics of *cF*8, *hP*8, and *hP*4. The difference of 0.8 kJ mol^{-1} Si^{-1} between the PBE0-D3 and LMP2 values is of similar magnitude to the differences between these methods for the low-density allotropes. There is no experimental thermodynamic data available for these silicon allotropes, but a recent study on the analogous *hP*8-Ge allotrope (4H-Ge) offers a point of comparison.[71] Using differential scanning calorimetry the transition enthalpy *hP*8-Ge → *cF*8-Ge was determined to be a value of 1.46 ± 0.55 kJ mol^{-1} Ge^{-1}. In the course of the present work we calculated the ΔE value of *hP*8-Ge at the PBE0-D3/TZVPP and LMP2/TZVPP levels of theory. Neglecting zero-point vibrational energy contributions, we obtained $\Delta E_{PBE0\text{-}D3}$ = 0.6 kJ mol^{-1} Ge^{-1} and ΔE_{LMP2} = 0.9 kJ mol^{-1} Ge^{-1}. Evidently, the LMP2 value is closer to the experimental value. This comparison suggests that the larger $\Delta E(hP8)$ and $\Delta E(hP4)$ values predicted for silicon by LMP2 are likely to be reasonable. We note that MP2 often overestimates dispersion interactions, this problem being the most severe for highly polarizable systems with a small band gap.[72]

Finally, we shortly comment on the energy ordering of the individual silicon allotropes obtained with various DFT approaches. We have carried out ΔE calculations also using the GGA functionals PBE and PBE-D3. The full results are not reported here since they do not really add any benefit beyond the already reported PBE0 and PBE0-D3 values, but we note that in general the predicted ΔE values increase as PBE < PBE0 < PBE-D3 < PBE0-D3. For example, for the lowest-density allotrope *cF*136, the predicted values increase as 6.1 < 7.2 < 10.8 < 12.6 kJ mol^{-1} Si^{-1}, the corresponding LMP2 value being 13.5 kJ mol^{-1} Si^{-1}. Based on this comparison, it appears that the dispersion interactions can be much more significant for the energy ordering of silicon allotropes than the use of a hybrid instead of the GGA functional. The data displayed in Fig. 4 also reveal the influence of the underlying PBE0 energies on the PBE0-D3 results: the latter curve has drops for the same structures as the PBE0 one, which are softened but not eliminated by the –D-contribution. In the LMP2 case such a bias is clearly absent.

It should be noted that while the ΔE values discussed here shed light on the relative stability of various silicon allotropes, it is not easy to transform the predicted ΔE values into successful guidelines for the experimental realization of novel silicon allotropes. In fact, while the diamond polytype allotropes *hP*8 and *hP*4 show very low relative energies in comparison to *cF*8, the bulk synthesis of neither allotrope has been realized. Instead, the *cF*136 and *oC*24 allotropes have been realized experimentally despite their rather high relative energy. Thus, when hunting for new silicon allotropes, it has so far proved to be more important to discover a suitable precursor material that can be modified to yield a metastable modification of silicon. For example, an important synthetic route towards novel silicon allotropes is *via* binary alkali metal phases such as Na_4Si_{24} and Na_xSi_{136}, from which the Na atoms can be removed with vacuum treatments in a controlled fashion to yield the new allotropes *oC*24 and *cF*136. Considering the predicted LMP2 and PBE0-D3 relative energies, it appears that even after taking the dispersion interactions into account, all hypothetical structures studied here could be experimentally feasible silicon allotropes, if suitable precursor materials can be discovered and there is a large enough energy barrier to prevent their immediate transformation into the *cF*8 structure or other more stable allotropes.

Conclusions

We have investigated how dispersion interactions affect the stability trends of the energetically most favorable silicon allotropes. Systematic calculations at the LMP2/TZVPP and PBE0-D3/TZVPP levels of theory clearly demonstrate that dispersion interactions in silicon networks can be so strong that the energy ordering of the allotropes is changed with respect

to DFT calculations not including dispersion interactions. Furthermore, inclusion of dispersion interactions can be much more significant for the energy ordering of silicon allotropes than the use of hybrid DFT instead of GGA-DFT. The LMP2/TZVPP calculations show that two experimentally known silicon allotropes, *oC*24 and *cF*136, possess rather high relative energies when the dispersion interactions are taken into account. Therefore, it appears that the denser and less strained silicon allotropes *hP*8, *hP*4, *oP*32, *tP*12, *hP*6, and *tP*24 should be feasible targets for experimental synthesis, provided that suitable precursor materials for them can be found.

Acknowledgements

A. J. K. gratefully acknowledges funding from the Alfred Kordelin Foundation. D. U. and M. S. acknowledge financial support from the Deutsche Forschungsgemeinschaft (Grants US-103/1-2 and SCHU-1456/12-1, respectively). The Finnish IT Center for Science (CSC) is thanked for providing the computing resources for this work. L. M. gratefully acknowledges support from the "Ricerca Locale 2015" funding of the university of Torino.

References

1 H. W. Kroto, J. R. Heath, S. C. O'Brien, R. F. Curl and R. E. Smalley, C60: Buckminsterfullerene, *Nature*, 1985, **318**, 162–163.
2 S. Iijima, Helical Microtubules of Graphitic Carbon, *Nature*, 1991, **354**, 56–58.
3 K. S. Novoselov, A. K. Geim, S. V. Morozov, D. Jiang, Y. Zhang, S. V. Dubonos, I. V. Grigorieva and A. A. Firsov, Electric Field in Atomically Thin Carbon Films, *Science*, 2004, **306**, 666–669.
4 J. Gryko, P. F. McMillan, R. F. Marzke, G. K. Ramachandran, D. Patton, S. K. Deb and O. F. Sankey, Low-Density Framework Form of Crystalline Silicon with a Wide Optical Band Gap, *Phys. Rev. B: Condens. Matter Mater. Phys.*, 2000, **62**, R7707.
5 A. Ammar, C. Cros, M. Pouchard, N. Jaussaud, J. Bassat, G. Villeneuve, M. Duttine, M. Ménétrier and E. Reny, On the Clathrate Form of Elemental Silicon, Si136: Preparation and Characterisation of NaxSi136 (X → 0), *Solid State Sci.*, 2004, **6**, 393–400.
6 D. Y. Kim, S. Stefanoski, O. O. Kurakevych and T. A. Strobel, Synthesis of an Open-Framework Allotrope of Silicon, *Nat. Mater.*, 2015, **14**, 169–173.
7 A. M. Guloy, R. Ramlau, Z. Tang, W. Schnelle, M. Baitinger and Y. Grin, A Guest-Free Germanium Clathrate, *Nature*, 2006, **443**, 320–323.
8 V. A. Blatov, M. O'Keeffe and D. M. Proserpio, Vertex-, Face-, Point-, Schläfli-, and Delaney-Symbols in Nets, Polyhedra and Tilings: Recommended Terminology, *CrystEngComm*, 2010, **12**, 44–48.
9 V. A. Blatov, A. P. Shevchenko and D. M. Proserpio, Applied Topological Analysis of Crystal Structures with the Program Package Topospro, *Cryst. Growth Des.*, 2014, **14**, 3576–3586.
10 M. O'Keeffe, M. A. Peskov, S. J. Ramsden and O. M. Yaghi, The Reticular Chemistry Structure Resource (RCSR) Database of, and Symbols for, Crystal Nets, *Acc. Chem. Res.*, 2008, **41**, 1782–1789.
11 R. Hoffmann, A. A. Kabanov, A. A. Golov and D. M. Proserpio, Homo Citans and Carbon Allotropes: For an Ethics of Citation, *Angew. Chem., Int. Ed.*, 2016, **55**, 10962–10976.
12 M. A. Zwijnenburg, K. E. Jelfs and S. T. Bromley, An Extensive Theoretical Survey of Low-Density Allotropy in Silicon, *Phys. Chem. Chem. Phys.*, 2010, **12**, 8505–8512.
13 A. J. Karttunen, T. F. Faessler, M. Linnolahti and T. A. Pakkanen, Structural Principles of Semiconducting Group 14 Clathrate Frameworks, *Inorg. Chem.*, 2011, **50**, 1733–1742.
14 L. A. Jantke, S. Stegmaier, A. J. Karttunen and T. F. Fässler, Slicing Diamond – A Guide to Deriving sp^3-Si Allotropes, *Chem. – Eur. J.*, 2017, **23**, 2734–2747.
15 A. Mujica, C. J. Pickard and R. J. Needs, Low-Energy Tetrahedral Polymorphs of Carbon, Silicon, and Germanium, *Phys. Rev. B: Condens. Matter Mater. Phys.*, 2015, **91**, 214104.
16 Z. Zhao, F. Tian, X. Dong, Q. Li, Q. Wang, H. Wang, X. Zhong, B. Xu, D. Yu, J. He, H. Wang, Y. Ma and Y. Tian, Tetragonal Allotrope of Group 14 Elements, *J. Am. Chem. Soc.*, 2012, **134**, 12362–12365.
17 J. C. Conesa, Computer Modeling of Allo-Si and Allo-Ge Polymorphs, *J. Phys. Chem. B*, 2002, **106**, 3402–3409.
18 M. M. J. Treacy, I. Rivin, E. Balkovsky, K. H. Randall and M. D. Foster, Enumeration of Periodic Tetrahedral Frameworks. II. Polynodal Graphs, *Microporous Mesoporous Mater.*, 2004, **74**, 121–132.
19 R. Pophale, P. A. Cheeseman and M. W. Deem, A Database of New Zeolite-Like Materials, *Phys. Chem. Chem. Phys.*, 2011, **13**, 12407–12412.
20 I. A. Baburin, D. M. Proserpio, V. A. Saleev and A. V. Shipilova, From Zeolite Nets to sp^3 Carbon Allotropes: A Topology-Based Multiscale Theoretical Study, *Phys. Chem. Chem. Phys.*, 2015, **17**, 1332–1338.
21 S. Grimme, Density Functional Theory with London Dispersion Corrections, *Wiley Interdiscip. Rev.: Comput. Mol. Sci.*, 2011, **1**, 211–228.
22 A. M. Reilly and A. Tkatchenko, van der Waals Dispersion Interactions in Molecular Materials: Beyond Pairwise Additivity, *Chem. Sci.*, 2015, **6**, 3289–3301.
23 M. Cutini, B. Civalleri, M. Corno, R. Orlando, J. G. Brandenburg, L. Maschio and P. Ugliengo, Assessment of Different Quantum Mechanical Methods for the Prediction of Structure and Cohesive Energy of Molecular Crystals, *J. Chem. Theory Comput.*, 2016, **12**, 3340–3352.
24 J. C. Conesa, The Relevance of Dispersion Interactions for the Stability of Oxide Phases, *J. Phys. Chem. C*, 2010, **114**, 22718–22726.
25 J. Moellmann, S. Ehrlich, R. Tonner and S. Grimme, A DFT-D Study of Structural and Energetic Properties of TiO_2 Modifications, *J. Phys.: Condens. Matter*, 2012, **24**, 424206.
26 M. Halo, C. Pisani, L. Maschio, S. Casassa, M. Schütz and D. Usvyat, Electron Correlation Decides the Stability of Cubic

Versus Hexagonal Boron Nitride, *Phys. Rev. B: Condens. Matter Mater. Phys.*, 2011, **83**, 035117.
27 M. Dion, H. Rydberg, E. Schrder, D. C. Langreth and B. I. Lundqvist, van der Waals Density Functional for General Geometries, *Phys. Rev. Lett.*, 2004, **92**, 246401.
28 A. Tkatchenko and M. Scheffler, Accurate Molecular van der Waals Interactions from Ground-State Electron Density and Free-Atom Reference Data, *Phys. Rev. Lett.*, 2009, **102**, 073005.
29 L. Schimka, J. Harl, A. Stroppa, A. Grneis, M. Marsman, F. Mittendorfer and G. Kresse, Accurate Surface and Adsorption Energies from Many-Body Perturbation Theory, *Nat. Mater.*, 2010, **9**, 741–744.
30 A. Tkatchenko, Current Understanding of van der Waals Effects in Realistic Materials, *Adv. Funct. Mater.*, 2015, **25**, 2054–2061.
31 G. Sansone, B. Civalleri, D. Usvyat, J. Toulouse, K. Sharkas and L. Maschio, Range-Separated Double-Hybrid Density-Functional Theory Applied to Periodic Systems, *J. Chem. Phys.*, 2015, **143**, 102811.
32 C. Pisani, M. Schütz, S. Casassa, D. Usvyat, L. Maschio, M. Lorenz and A. Erba, CRYSCOR: A Program for the Post-Hartree-Fock Treatment of Periodic Systems, *Phys. Chem. Chem. Phys.*, 2012, **14**, 7615–7628.
33 M. Del Ben, J. Hutter and J. Vandevondele, Second-Order Moller-Plesset Perturbation Theory in the Condensed Phase: An Efficient and Massively Parallel Gaussian and Plane Waves Approach, *J. Chem. Theory Comput.*, 2012, **8**, 4177–4188.
34 J. Paier, X. Ren, P. Rinke, G. E. Scuseria, A. Grneis, G. Kresse and M. Scheffler, Assessment of Correlation Energies Based on the Random-Phase Approximation, *New J. Phys.*, 2012, **14**, 043002.
35 M. Del Ben, J. Hutter and J. Vandevondele, Electron Correlation in the Condensed Phase from a Resolution of Identity Approach Based on the Gaussian and Plane Waves Scheme, *J. Chem. Theory Comput.*, 2013, **9**, 2654–2671.
36 H. Stoll, On the Correlation Energy of Graphite, *J. Chem. Phys.*, 1992, **97**, 8449–8454.
37 B. Paulus, The Method of Increments - A Wavefunction-Based Ab Initio Correlation Method for Solids, *Phys. Rep.*, 2006, **428**, 1–52.
38 D. Usvyat, K. Sadeghian, L. Maschio and M. Schütz, Geometrical Frustration of an Argon Monolayer Adsorbed on the MgO (100) Surface: An Accurate Periodic *Ab Initio* Study, *Phys. Rev. B: Condens. Matter Mater. Phys.*, 2012, **86**, 045412.
39 D. Usvyat, High Precision Quantum-Chemical Treatment of Adsorption: Benchmarking Physisorption of Molecular Hydrogen on Graphane, *J. Chem. Phys.*, 2015, **143**, 104704.
40 G. Sansone, L. Maschio, D. Usvyat, M. Schütz and A. Karttunen, Toward an Accurate Estimate of the Exfoliation Energy of Black Phosphorus: A Periodic Quantum Chemical Approach, *J. Phys. Chem. Lett.*, 2016, **7**, 131–136.
41 J. Yang, W. Hu, D. Usvyat, D. Matthews, M. Schütz and G. K. Chan, Ab Initio Determination of the Crystalline Benzene Lattice Energy to Sub-Kilojoule/Mole Accuracy, *Science*, 2014, **345**, 640–643.
42 R. Martinez-Casado, D. Usvyat, L. Maschio, G. Mallia, S. Casassa, J. Ellis, M. Schütz and N. M. Harrison, Approaching an Exact Treatment of Electronic Correlations at Solid Surfaces: The Binding Energy of the Lowest Bound State of Helium Adsorbed on MgO(100), *Phys. Rev. B: Condens. Matter Mater. Phys.*, 2014, **89**, 205138.
43 D. Usvyat, L. Maschio and M. Schütz, Periodic Local MP2 Method Employing Orbital Specific Virtuals, *J. Chem. Phys.*, 2015, **143**, 102805.
44 A. J. Karttunen and T. F. Fässler, Semiconducting Clathrates Meet Gas Hydrates: Xe24[Sn136], *Chem. – Eur. J.*, 2014, **20**, 6693–6698.
45 C. Pisani, M. Busso, G. Capecchi, S. Casassa, R. Dovesi, L. Maschio, C. Zicovich-Wilson and M. Schütz, Local-MP2 Electron Correlation Method for Nonconducting Crystals, *J. Chem. Phys.*, 2005, **122**, 094113.
46 R. Dovesi, R. Orlando, A. Erba, C. M. Zicovich-Wilson, B. Civalleri, S. Casassa, L. Maschio, M. Ferrabone, M. De La Pierre, P. D'Arco, Y. Noël, M. Causà, M. Rérat and B. Kirtman, CRYSTAL14: A Program for the Ab Initio Investigation of Crystalline Solids, *Int. J. Quantum Chem.*, 2014, **114**, 1287–1317.
47 J. P. Perdew, K. Burke and M. Ernzerhof, Generalized Gradient Approximation made Simple, *Phys. Rev. Lett.*, 1996, **77**, 3865–3868.
48 C. Adamo and V. Barone, Toward Reliable Density Functional Methods without Adjustable Parameters: The PBE0 Model, *J. Chem. Phys.*, 1999, **110**, 6158–6170.
49 S. Grimme, J. Antony, S. Ehrlich and H. Krieg, A Consistent and Accurate Ab Initio Parametrization of Density Functional Dispersion Correction (DFT-D) for the 94 Elements H-Pu, *J. Chem. Phys.*, 2010, **132**, 154104.
50 S. Grimme, S. Ehrlich and L. Goerigk, Effect of the Damping Function in Dispersion Corrected Density Functional Theory, *J. Comput. Chem.*, 2011, **32**, 1456–1465.
51 F. Weigend and R. Ahlrichs, Balanced Basis Sets of Split Valence, Triple Zeta Valence and Quadruple Zeta Valence Quality for H to Rn: Design and Assessment of Accuracy, *Phys. Chem. Chem. Phys.*, 2005, **7**, 3297–3305.
52 H. J. Monkhorst and J. D. Pack, Special Points for Brillouin-Zone Integrations, *Phys. Rev. B: Condens. Matter Mater. Phys.*, 1976, **13**, 5188–5192.
53 T. Risthaus and S. Grimme, Benchmarking of London Dispersion-Accounting Density Functional Theory Methods on very Large Molecular Complexes, *J. Chem. Theory Comput.*, 2013, **9**, 1580–1591.
54 M. Schütz, D. Usvyat, M. Lorenz, C. Pisani, L. Maschio, S. Casassa and M. Halo, in *Accurate Condensed-Phase Quantum Chemistry, Computation in Chemistry*, ed. Frederick R. Manby, CRC Press, 2010, vol. 27.
55 F. R. Manby, P. J. Knowles and A. W. Lloyd, The Poisson Equation in Density Fitting for the Kohn-Sham Coulomb Problem, *J. Chem. Phys.*, 2001, **115**, 9144–9148.
56 L. Maschio, D. Usvyat, F. R. Manby, S. Casassa, C. Pisani and M. Schütz, Fast Local-MP2 Method with Density-Fitting for Crystals. I. Theory and Algorithms, *Phys. Rev. B: Condens. Matter Mater. Phys.*, 2007, **76**, 075101.

57 F. Weigend, M. Haeser, H. Patzelt and R. Ahlrichs, RI-MP2: Optimized Auxiliary Basis Sets and Demonstration of Efficiency, *Chem. Phys. Lett.*, 1998, **294**, 143–152.

58 M. E. Straumanis and E. Z. Aka, Lattice Parameters, Coefficients of Thermal Expansion, and Atomic Weights of Purest Silicon and Germanium, *J. Appl. Phys.*, 1952, **23**, 330–334.

59 D. N. Batchelder and R. O. Simmons, Lattice Constants and Thermal Expansivities of Silicon and of Calcium Fluoride between 6 and 322K, *J. Chem. Phys.*, 1964, **41**, 2324–2329.

60 F. Ortmann, F. Bechstedt and W. G. Schmidt, Semiempirical van der Waals Correction to the Density Functional Description of Solids and Molecular Structures, *Phys. Rev. B: Condens. Matter Mater. Phys.*, 2006, **73**, 205101.

61 C. He, C. Zhang, J. Li, X. Peng, L. Meng, C. Tang and J. Zhong, Direct and Quasi-Direct Band Gap Silicon Allotropes with Remarkable Stability, *Phys. Chem. Chem. Phys.*, 2016, **18**, 9682–9686.

62 F. Kiefer, V. Hlukhyy, A. J. Karttunen, T. F. Faessler, C. Gold, E. Scheidt, W. Scherer, J. Nylen and U. Haeussermann, Synthesis, Structure, and Electronic Properties of 4H-Germanium, *J. Mater. Chem.*, 2010, **20**, 1780–1786.

63 F. Kiefer, A. J. Karttunen, M. Doeblinger and T. F. Faessler, Bulk Synthesis and Structure of a Microcrystalline Allotrope of Germanium (M-Allo-Ge), *Chem. Mater.*, 2011, **23**, 4578–4586.

64 H. I. T. Hauge, M. A. Verheijen, S. Conesa-Boj, T. Etzelstorfer, M. Watzinger, D. Kriegner, I. Zardo, C. Fasolato, F. Capitani, P. Postorino, S. Kölling, A. Li, S. Assali, J. Stangl and E. P. A. M. Bakkers, Hexagonal Silicon Realized, *Nano Lett.*, 2015, **15**, 5855–5860.

65 L. Öhrström and M. O'Keeffe, Network Topology Approach to New Allotropes of the Group 14 Elements, *Z. Kristallogr.*, 2013, **288**, 343–346.

66 C. J. Pickard and R. J. Needs, Hypothetical Low-Energy Chiral Framework Structure of Group 14 Elements, *Phys. Rev. B: Condens. Matter Mater. Phys.*, 2010, **81**, 14106.

67 M. Zeilinger, L. Vanwüllen, D. Benson, V. F. Kranak, S. Konar, T. F. Fässler and U. Häussermann, LiBSi2: A Tetrahedral Semiconductor Framework from Boron and Silicon Atoms Bearing Lithium Atoms in the Channels, *Angew. Chem., Int. Ed.*, 2013, **52**, 5978–5982.

68 D. Y. Kim, S. Stefanoski, O. O. Kurakevych and T. A. Strobel, Synthesis of an Open-Framework Allotrope of Silicon, *Nat. Mater.*, 2015, **14**, 169–173.

69 A. Shevelkov and K. Kovnir, Zintl Clathrates, *Struct. Bonding*, 2011, **139**, 97–142.

70 J. Dolyniuk, B. Owens-Baird, J. Wang, J. V. Zaikina and K. Kovnir, Clathrate Thermoelectrics, *Mater. Sci. Eng., R*, 2016, **108**, 1–46.

71 J. V. Zaikina, E. Muthuswamy, K. I. Lilova, Z. M. Gibbs, M. Zeilinger, G. J. Snyder, T. F. Fässler, A. Navrotsky and S. M. Kauzlarich, Thermochemistry, Morphology, and Optical Characterization of Germanium Allotropes, *Chem. Mater.*, 2014, **26**, 3263–3271.

72 M. Schütz, L. Maschio, A. J. Karttunen and D. Usvyat, The Exfoliation Energy of Black Phosphorus Revisited: A Coupled Cluster Benchmark, *J. Phys. Chem. Lett.*, 2017, DOI: 10.1021/acs.jpclett.7b00253.